

A Game-Theoretic Spatio-Temporal Reinforcement Learning Framework for Collaborative Public Resource Allocation

Songxin Lei^{1*}, Qiongyan Wang^{1*}, Yanchen Zhu¹, Hanyu Yao², Sijie Ruan³,
Weilin Ruan¹, Yuyu Luo¹, Huaming Wu⁴, Yuxuan Liang^{1†}

¹The Hong Kong University of Science and Technology (Guangzhou)

²Peking University ³Beijing Institute of Technology ⁴Tianjin University

{slei924, qwang650, yzhu156, wruan792} @connect.hkust-gz.edu.cn; 2501112585@stu.pku.edu.cn;
sruan@bit.edu.cn; yuyuluo@hkust-gz.edu.cn; whming@tju.edu.cn; yuxliang@outlook.com

Abstract

Public resource allocation involves the efficient distribution of resources, including urban infrastructure, energy, and transportation, to effectively meet societal demands. However, existing methods focus on optimizing the movement of individual resources independently, without considering their capacity constraints. To address this limitation, we propose a novel and more practical problem: Collaborative Public Resource Allocation (CPRA), which explicitly incorporates capacity constraints and spatio-temporal dynamics in real-world scenarios. We propose a new framework called Game-Theoretic Spatio-Temporal Reinforcement Learning (GSTRL) for solving CPRA. Our contributions are twofold: 1) We formulate the CPRA problem as a potential game and demonstrate that there is no gap between the potential function and the optimal target, laying a solid theoretical foundation for approximating the Nash equilibrium of this NP-hard problem; and 2) Our designed GSTRL framework effectively captures the spatio-temporal dynamics of the overall system. We evaluate GSTRL on two real-world datasets, where experiments show its superior performance.

Introduction

Effective public resource allocation is a cornerstone of equitable and resilient urban development. From emergency response (Feng and Xiao 2024) and disaster relief (Wang et al. 2021) to mobile healthcare (Liu et al. 2024) and traffic control (Ji, Zheng, and Li 2016), the ability to dynamically deploy limited resources directly impacts the safety, well-being, and quality of life of millions of residents. In particular, underserved communities, high-density zones, and vulnerable populations are disproportionately affected by inefficiencies in service delivery (Yang et al. 2024). As cities grow increasingly complex and demand fluctuates across space and time, traditional static or heuristic-based systems fall short in meeting these critical needs.

To ensure responsive and inclusive service delivery, *dynamic public resource allocation* is emerging as a vital AI-enabled mechanism for optimizing operational effi-

*These authors contributed equally.

†Corresponding author. E-mail: yuxliang@outlook.com

Copyright © 2026, Association for the Advancement of Artificial Intelligence (www.aaai.org). All rights reserved.

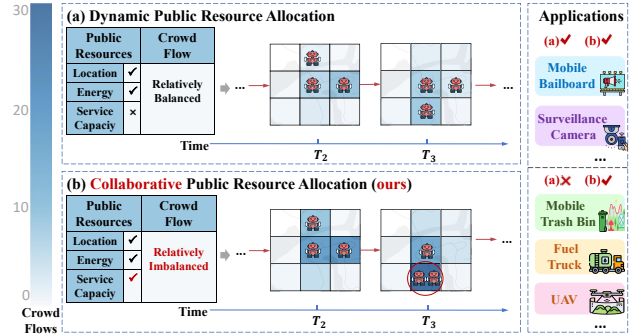


Figure 1: Dynamic public resource allocation vs. Collaborative public resource allocation (CPRA).

ciency under uncertainty (Liu et al. 2022). Yet, as shown in **Fig. 1**, real-world deployment remains highly challenging: resources are limited in capacity, demands are volatile and spatially clustered, so that coordination among resources to serve a single region in special cases is necessary to prevent overload or neglect (Lv et al. 2024). These factors underscore the urgency of developing principled and scalable approaches that can reason about cooperation, adapt to changing conditions, and ultimately improve social outcomes.

Unfortunately, most existing AI-based approaches to dynamic allocation treat each resource independently, assuming either unlimited capacities or neglecting the alignment between the individual and the system (Ruan et al. 2020). Such simplifications fail to capture the collaborative nature of real-world systems, where multiple limited-capacity resources must jointly serve emerging high-demand areas (Sadeghi Eshkevari et al. 2022). For example, during peak hours or emergencies, a single ambulance or mobile testing unit is rarely sufficient (Ji et al. 2019). This reveals two key requirements for effective dynamic allocation: the need for *capacity-aware optimization* and the need for *co-operative decision-making*.

To bridge this gap, we introduce the Collaborative Public Resource Allocation (CPRA) problem as shown in **Fig. 1**, which explicitly models the capacity constraints and spatio-temporal dynamics in real-world public resource systems.

Compared to dynamic public resource allocation, CPRA involves a more complex state space, presenting two core challenges: (i) how to enable effective joint scheduling among all resources without falling into suboptimal solutions; and (ii) how to capture complex spatio-temporal demand dynamics for proactive, high-coverage decision-making.

To address these challenges, we propose a new framework called Game-Theoretic Spatio-Temporal Reinforcement Learning (GSTRL) for solving CPRA. Targeting the first challenge, we prove that the CPRA problem can be formulated as a *Potential Game*, and then guide the reward learning rule for the system based on potential function, providing theoretical guarantees that aligning individual incentives can achieve socially optimal outcomes. To tackle the second challenge, GSTRL integrates a spatio-temporal demand forecasting module and adaptive policy learning, enabling dispatch strategies under real-world constraints. Our major contributions can be summarized as follows:

- *A novel perspective from the game theory*: To the best of our knowledge, we are the first to introduce the CPRA problem, considering *capacity constraints* and *agent collaboration*. By formulating it as a potential game model with a constructed potential function to capture collaboration dynamics, we provide theoretical guarantees for accelerating convergence towards a near-Nash equilibrium.
- *A new framework for CPRA*: We propose GSTRL, a reinforcement learning (RL) framework to solve the CPRA problem. By leveraging dynamically updated and incorporating a series of feature extraction components, GSTRL effectively captures *spatio-temporal dynamics* from predicted crowd flow and public resources.
- *Comprehensive empirical evidence*: Extensive experiments on two real-world datasets show that GSTRL outperforms state-of-the-art baselines by up to 40%, demonstrating its superior performance on the CPRA problem across various parameter settings. Ablation and convergence experiments further highlight the role of its key components in enhancing learning effectiveness.

Overview

In this section, we give some preliminaries, then we formally define CPRA and prove its NP-hardness for the first time.

Preliminaries

Definition 1 (Location). *We uniformly partition the area of interest into N grid locations, denoted by $\mathcal{G} = \{g_i\}$.*

Definition 2 (Public Resource). *At any time interval T_t , the resource \mathbf{m}_k is represented as a triple $\mathbf{m}_t = (l_k^t, e_k^t, p_k^t)$, where $l_k^t \in \mathcal{G}$ denotes its current location, e_k^t represents its remaining energy, and p_k^t indicates its service capacity.*

Definition 3 (Energy Cost). *When a resource moves from g_i to g_j , the energy cost is denoted by $c_{i,j}$. We treat all resources of the same type, making energy cost solely dependent on Euclidean travel distance (Ruan et al. 2020).*

Definition 4 (Service Capacity). *The service capacity of a resource k at time t , denoted by p_k^t , measures the crowd flow that the resource can serve at time t . We assume that the*

service capacity is identical for all resources and is updated at each time step, such that $p_k^{t+1} = p_k^t = p_{k+1}^t$.

Definition 5 (Resource Depot). *A resource depot $g_\omega \in \mathcal{G}$ is static. All public resources must start and end their journey at this resource depot during the scheduling process.*

Definition 6 (Crowd Coverage). *The crowd coverage during the time interval T_t is defined as the total number of people successfully served by all public resources across the entire area. Let $u_{i,k}^t$ indicate the presence of public resource m_k in grid cell i at time t , and let λ_i^t represent the crowd flow in grid i at time t . Consequently, the crowd coverage during the time interval T_t can be expressed as:*

$$C_t = \sum_{k \in \mathcal{K}} \sum_{g_i \in \mathcal{G}} (u_{i,k}^t \cdot \min \{\lambda_i^t, p_k^t\}). \quad (1)$$

Problem Statement

Given a set of public resources $\mathcal{K} = \{k = 1, \dots, k_{\max}\}$, a set of service time intervals $\mathcal{T} = \{T_t \mid t = 1, \dots, t_{\max}\}$, an initial energy E , and the location of the resource depot g_ω , our objective is to find a scheduling strategy that maximizes long-term crowd coverage while adhering to energy limits and ensuring that all public resources start and end their journeys at the resource depot. Since most resources operate in fixed positions, decision-making time dominates travel time, which is thus neglected.

Based on crowd flow distributions, this optimization problem is formulated as an Integer Linear Programming (ILP) problem with respect to the decision variable $u_{i,k}^t$. To facilitate the solution, we introduce an auxiliary variable $x_{i,j,k}^t$, which indicates whether resource m_k travels from location g_i to location g_j at the beginning of T_t :

$$\sum_{g_h \in \mathcal{G}} x_{h,i,k}^t = \sum_{g_j \in \mathcal{G}} x_{i,j,k}^{t+1} = u_{i,k}^t, \forall g_i \in \mathcal{G}, T_t \in \mathcal{T}, k \in \mathcal{K}. \quad (2)$$

The formulation of CPRA is expressed as follows:

$$\mathcal{P} : \max_{\{u_{i,k}^t\}} \sum_{t \in \mathcal{T}} \sum_{k \in \mathcal{K}} \sum_{g_i \in \mathcal{G}} (u_{i,k}^t \cdot \min \{\lambda_i^t, p_k^t\}) \quad (3)$$

$$s.t. \quad C_1 : \sum_{k \in \mathcal{K}} \sum_{g_i \in \mathcal{G} \setminus \{g_\omega\}, g_j \in \mathcal{G}} x_{i,j,k}^t = 0, \quad (3a)$$

$$C_2 : \sum_{k \in \mathcal{K}} \sum_{g_j \in \mathcal{G}} x_{\omega,j,k}^1 = \sum_{k \in \mathcal{K}} \sum_{g_i \in \mathcal{G}} x_{i,\omega,k}^{n+1} = k_{\max}, \quad (3b)$$

$$C_3 : \sum_{k \in \mathcal{K}} u_{i,k}^t \leq \frac{\sum_{g_i \in \mathcal{G}} \lambda_i^t}{p_k^t}, \forall g_i \in \mathcal{G}, T_t \in \mathcal{T}, \quad (3c)$$

$$C_4 : \sum_{t \in \mathcal{T} \cup \{t_{n+1}\}} \sum_{g_i, g_j \in \mathcal{G}} c_{i,j} \cdot x_{i,j,k}^t \leq E, \forall k \in \mathcal{K}, \quad (3d)$$

where constraint C_1 ensures all routes start from the resource depot g_ω . C_2 enforces that each resource starts and ends at g_ω , occupying a location at both T_1 and $T_{t_{\max}}$. C_3 limits the number of resources in g_i at time T_t , preventing trivial stationary solutions. C_4 ensures each resource has sufficient energy E to return to the depot.

Theorem 1. *The CPRA problem \mathcal{P} is NP-hard.*

Due to space limitations, we provide the proof in **Appendix**, where we demonstrate that the CPRA problem \mathcal{P} is computationally intractable, underscoring the need for advanced algorithmic approaches.

A Game-Theoretic View on CPRA

To design an effective algorithm for the NP-hard CPRA problem, we analyze the relationship between individual agents and the overall system in CPRA from the perspective of potential game theory.

Potential Game Model

We treat each public resource as a player and the combination of resources and crowd flow as a system, the CPRA problem is modeled as a game $G = \{\mathcal{K}, \mathcal{S}, \{U_k\}_{k \in \mathcal{K}}\}$:

- \mathcal{K} is the set of players (public resources).
- $\mathcal{S} = S_1 \times S_2 \times \dots \times S_{k_{max}}$ represents the joint strategy space of the game, with S_k being the set of all possible strategies for public resource m_k .
- U_k is the utility function of public resource m_k .

Each strategy profile $\zeta \in \mathcal{S}$ is defined as $\zeta = (\zeta_1, \zeta_2, \dots, \zeta_{k_{max}})$, which can also be expressed as $\zeta = (\zeta_k, \zeta_{-k})$, where ζ_{-k} represents the strategies of all resources except m_k . The goal of each resource is to maximize its utility $U_k(\zeta)$ based on the allocation strategy.

Definition 7 (Utility function of public resource m_k). *The utility of public resource m_k under strategy ζ is defined as the sum of the crowd coverage achieved at time t :*

$$U_k(\zeta) = \sum_{g_i \in \mathcal{G}} (u_{i,k}^t \cdot \min \{\lambda_i^t, p_k^t\}). \quad (4)$$

Definition 8 (Potential Game). *A game $G = \{\mathcal{K}, \mathcal{S}, \{U_k\}_{k \in \mathcal{K}}\}$ is a **potential game** if there exists a potential function $\Phi : \mathcal{S} \rightarrow \mathbb{R}$ such that for all $k \in \mathcal{K}$, all $\zeta_{-k} \in S_{-k}$, and all $\zeta_k, \zeta'_k \in S_k$,*

$$U_k(\zeta_k, \zeta_{-k}) - U_k(\zeta'_k, \zeta_{-k}) = \Phi(\zeta_k, \zeta_{-k}) - \Phi(\zeta'_k, \zeta_{-k}).$$

Theorem 2. *The game $G = \{\mathcal{K}, \mathcal{S}, \{U_k\}_{k \in \mathcal{K}}\}$ is a potential game with the potential function:*

$$\Phi(\zeta) = \sum_{k \in \mathcal{K}} \sum_{g_i \in \mathcal{G}} (u_{i,k}^t \cdot \min \{\lambda_i^t, p_k^t\}). \quad (5)$$

Proof. The potential function $\Phi(\zeta)$ is defined as the total crowd coverage achieved by all public resources:

$$\Phi(\zeta) = \sum_{k \in \mathcal{K}} U_k(\zeta) = \sum_{k \in \mathcal{K}} \sum_{g_i \in \mathcal{G}} (u_{i,k}^t \cdot \min \{\lambda_i^t, p_k^t\}).$$

Now, consider the change in the strategy of a single resource m_k from ζ_k to ζ'_k , while all other strategies ζ_{-k} remain fixed. The resulting change in the potential function is:

$$\Phi(\zeta_k, \zeta_{-k}) - \Phi(\zeta'_k, \zeta_{-k}) = U_k(\zeta_k, \zeta_{-k}) - U_k(\zeta'_k, \zeta_{-k}).$$

This confirms that the difference in the potential function directly reflects the change in the utility of the public resource m_k , satisfying the conditions for a potential game. \square

Theorem 3. *Every finite potential game has at least one pure-strategy Nash equilibrium.*

Due to space limit, we leave the proof in **Appendix**.

Further Discussion

Guided by **Theorem 3**, we employ a RL algorithm to address this NP-hard problem. We adopt the potential function as the reward function, establishing theoretical guarantees for the algorithm's convergence and capacity to approximate the optimal solution.

For the CPRA problem, we further demonstrate that there exists no gap between the optimal objective and the Nash equilibrium. From a system-level perspective, this ensures that maximizing each player's utility inherently maximizes overall system performance, leading to no resource redundancy. From a decision-making perspective, this alignment implies that information sharing does not introduce bias. Motivated by these insights, we adopt a centralized decision-making framework in which the entire system learns an optimal strategy under a unified reward structure.

Methodology

Framework Overview

Given a distribution of crowd flows and resources, our goal is to design allocation strategies that maximize long-term coverage by placing resources in the optimal locations at each time step. **Fig. 2** illustrates the framework, which mainly consists of three modules:

- **Initial State Embedding:** This module is divided into two components: crowd flow embedding and agent embedding. First, we flatten the predicted flows and use an MLP layer to process the initial state of public resources (Wang et al. 2025). Then, a Stem and LayerNorm component is applied to extract high-level features (denoted as \mathbf{X}_t and \mathbf{Y}_t), where $t \in \{t_1, t_2, \dots, t_{max}\}$.
- **Spatio-Temporal Feature Extraction:** Starting with the crowd flow embedding output X_t , this module uses three Bidirectional LSTMs and a Fourier Neural Operator to capture the spatial and temporal dynamics of X_t . The spatial feature S^t and temporal feature T_t are then concatenated as R_t for further processing.
- **Allocation Decision Making:** We first apply a gating mechanism to integrate the spatio-temporal embedding of predicted flows R_t with the public resources embedding Y_t , followed by a mask criterion to ensure the strategies comply with practical constraints. A softmax layer is then used to calculate the score for each action Q_k , which is executed accordingly.

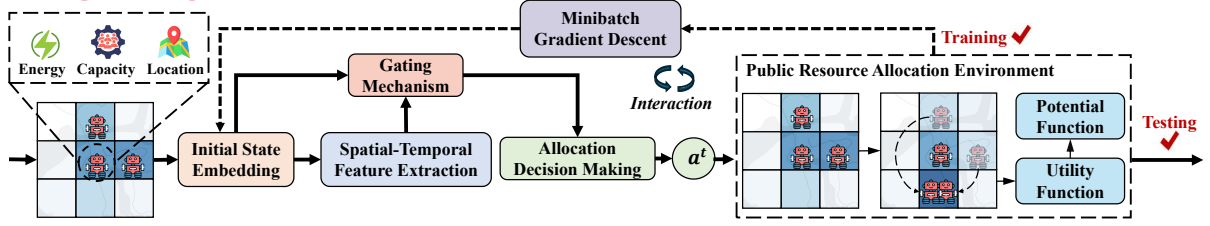
During training, agents interact with the environment and get experience. We sample mini-batches from the experience and refine the strategy using mini-batch gradient descent until convergence (Qi et al. 2023).

CPRA Modeled as Markov Decision Process

To capture long-term effects and avoid myopic decisions, we formulate the resource allocation process as a Markov Decision Process (MDP). It consists of four components: states, actions, transitions, and rewards.

a) State. We denote the state at time t by $s_t = (\mathbf{d}_t, \mathcal{M}_t)$, where $\mathbf{d}_t = \{\lambda_i^t\}_{g_i \in \mathcal{G}}$ is the set of predicted flows in each grid, and $\mathcal{M}_t = \{(l_k^t, e_k^t, p_k^t)\}_{k=1}^{k_{max}}$ is the set of resources.

Training & Testing Process



Network Structure of Three Key Modules

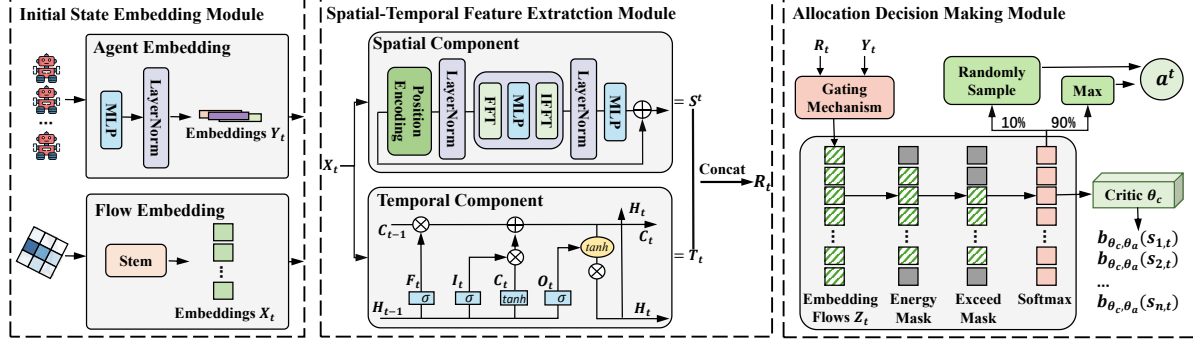


Figure 2: Overall architecture of the proposed GSTRL framework.

b) Action. At time step t , the action $a_t = (g_i^t, \mathbf{m}_k^t)$ means that we allocate resource \mathbf{m}_k to grid g_i .

c) Transitions. Once an action a_t is taken, the system deterministically transitions to s_{t+1} based on s_t and a_t .

d) Reward. Based on potential game theory, we adopt the potential function $\Phi(\zeta)$ as the reward function, which is $r_t = \sum_{k \in \mathcal{K}} \sum_{g_i \in \mathcal{G}} (u_{i,k}^t \cdot \min\{\lambda_i^t, p_k^t\})$ at time t . By using a global optimization function instead of individual utility functions for each resource, GSTRL can capture the agent collaboration dynamics more effectively so as to accelerate convergence toward a near-Nash equilibrium.

Initial State Embedding

We design an Initial State Embedding Module to convert predicted crowd flows and resource states into high-level features for subsequent learning. This involves two parts: Crowd Flow Embedding and Agent Embedding.

Flow Embedding. Input data reflects the dynamics of crowd flows. After flattening, we feed the data into a stem module with 1×1 convolutions to extract a feature map \mathbf{X}_t .

Agent Embedding. Each resource is denoted by (l_k^t, e_k^t, p_k^t) . We project the 3-dimensional vector into a higher-dimensional space via a fully connected layer, followed by LayerNorm. We denote the preliminary embedding resulting from each public resource by \mathbf{Y}_t .

Spatio-Temporal Feature Extraction

Our module refines the features from the Crowd Flow Embedding via two main components: a Temporal Component and a Spatial Component.

Temporal Component. We adopt a BiLSTM (Schuster and Paliwal 1997) to capture long-term temporal patterns

in crowd flow. Unlike unidirectional models, BiLSTM processes each time step in both forward and backward directions. This process yields hidden states $\vec{\mathbf{H}}_t$ and $\overleftarrow{\mathbf{H}}_t$. Concatenating them produces a comprehensive temporal embedding \mathbf{T}_t , which helps avoid suboptimal dispatching (Hu et al. 2024b,a). We leave the details in **Appendix**.

Spatial Component. We adopt FNO (Li et al. 2021) to capture global correlations in the frequency domain with reduced complexity. Let $\mathbf{X}_t \in \mathbb{R}^{N \times E}$ denote the spatial feature map at time t . After position encoding and LayerNorm, we transform \mathbf{X}_t via FFT, multiply by a learnable weight matrix $\hat{\mathbf{W}}$, and apply the inverse FFT:

$$\mathbf{s}_i^t = \text{IFFT}(\hat{\mathbf{W}} \cdot \text{FFT}(\mathbf{X}_t))_i, \quad (6)$$

where i indexes the grids, and the structure of $\hat{\mathbf{W}}$ reduces parameter count. This yields spatial embeddings $\mathbf{S}^t = \{\mathbf{s}_1^t, \dots, \mathbf{s}_N^t\}$ in $\mathcal{O}(NE \log N)$ time, where N is the number of grids and E the embedding dimension.

Output. We concatenate \mathbf{T}_t and \mathbf{S}^t to form the spatio-temporal embedding $\mathbf{R}_t = \text{Concat}(\mathbf{T}_t, \mathbf{S}^t)$, which captures both time-series trends and cross-grid interactions. \mathbf{R}_t is then passed to the Allocation Decision Making Module, enabling resource allocation under capacity constraints and fluctuating demands (Liang et al. 2021).

Allocation Decision Making

This module integrates the spatio-temporal embedding \mathbf{R}_t and the resource embedding \mathbf{Y}_t via a gating mechanism:

$$\mathbf{J}_t = \sigma(\mathbf{W}_j \cdot [\mathbf{R}_t, \mathbf{Y}_t] + \mathbf{b}_j), \mathbf{Z}_t = \mathbf{J}_t \cdot \mathbf{R}_t + (1 - \mathbf{J}_t) \cdot \mathbf{Y}_t, \quad (7)$$

where \mathbf{W}_j and \mathbf{b}_j are learnable parameters, and $\sigma(\cdot)$ is the sigmoid function. The resulting \mathbf{Z}_t represents the overall feature for the system for subsequent decision-making.

When making decisions, the four constraints C_1 – C_4 must be satisfied. Although C_1 and C_2 are effective by design, C_3 and C_4 require restricting locations based on the state of each resource. We thus apply masking mechanisms to \mathbf{Z}_t , yielding a masked representation $\overline{\mathbf{Z}}_t$.

Finally, We decode $\overline{\mathbf{Z}}_t$ through a softmax layer $\mathbf{Q}_k = \text{Softmax}(\overline{\mathbf{Z}}_t)$. During training, the agent chooses the highest-probability action 90% of the time and randomly explores 10% of the time. The processed state is also passed to the Critic module $b_{\theta_c, \theta_a}(s_{i,t})$ for value estimation.

Training Process

To learn an effective allocation strategy, we adopt an Actor-Critic training framework (Mao et al. 2023). The procedural flow of the training process is depicted in **Appendix**.

Actor-Critic Overview. Our Actor-Critic method comprises two main components:

- **Actor (Policy Network):** The policy network, denoted as π_{θ_a} , governs resource allocation decisions of GSTRL. The Initial State Embedding Module, Spatio-Temporal Feature Extraction Module, and Allocation Decision Module are essential components of the policy network.
- **Critic (Value Network):** The value network approximates the value function $V_{\pi_{\theta_a}}(s_t)$, which evaluates state quality and guides the Actor towards higher-value actions. Implemented as a feed-forward network with a regression layer and parameterized by θ_c , the value network is trained alongside the Actor network but is not used after training.

By integrating these two components, GSTRL dynamically optimizes allocation strategies using mini-batch gradient descent. We leave the details of the definition of value functions and advantage in **Appendix**.

Loss Functions. The Critic is optimized via:

$$\mathcal{L}_{\theta_c} = \frac{1}{N} \sum_{i=1}^N \sum_{t \in \mathcal{T}} \text{smoothL1}(b_{\theta_c, \theta_a}(s_{i,t}) - r_{i,t}), \quad (8)$$

where the predicted value $b_{\theta_c, \theta_a}(s_{i,t})$ is defined as a baseline to evaluate the value function. The Actor is trained to maximize the expected advantage:

$$\mathcal{L}_{\theta_a} = \frac{1}{N} \sum_{i=1}^N \sum_{t \in \mathcal{T}} \log \pi_{\theta_a}(a_{i,t} | s_{i,t}) A_{\pi_{\theta_a}}(s_{i,t}, a_{i,t}), \quad (9)$$

where N denotes the number of sampled trajectories, π_{θ_a} is the policy, and $A_{\pi_{\theta_a}}(\cdot)$ is the advantage function. We train the Actor and Critic jointly by combining their losses:

$$\mathcal{L}_{\theta_{ac}} = \alpha \mathcal{L}_{\theta_a} + \beta \mathcal{L}_{\theta_c}, \quad (10)$$

where α and β are hyperparameters controlling the trade-off between policy optimization and value estimation.

Experiments

Experimental Settings

Datasets. We utilize two datasets, Happy Valley and TaxiBJ, for our capacitated resource scheduling task.

- **Happy Valley:** This dataset, obtained from Ruan et al. (Ruan et al. 2020), provides hourly gridded crowd flow observations for Beijing Happy Valley, a theme park covering $1.25 \times 10^5 m$. The data spans from January 1, 2018, to October 31, 2018. We divide the park into a 51×108 grid for fine-grained analysis. The dataset is split into training (60%), validation (20%), and test (20%) sets.
- **TaxiBJ:** This dataset, published by Zhang et al. (Zhang, Zheng, and Qi 2017), records taxi flow data across Beijing from July 1, 2013, to March 31, 2016. We represent the city as a 32×32 grid to model the spatial distribution of taxi movements. The dataset is partitioned into 70% for training, 20% for validation, and 10% for testing.

Baselines & Evaluation Metrics. To evaluate the CPRA problem, we implement several heuristic algorithms, such as Static, B&B (Lawler and Wood 1966), MYOPIC (Ruan et al. 2020), and EADS (Ruan et al. 2020). Besides, as we are the first to study CPRA, we adapt state-of-the-art RL algorithms from related domains, such as REINFORCE (Zhang et al. 2020), PPO (Zhu, Zheng, and Jamalipour 2025), SAC (Zheng, Kurt, and Wang 2024), HEM (Wang et al. 2024), for a comprehensive comparison. Notably, since each resource’s state and action are independent, modeling them as individual agents in multi-agent RL would require local observations, which contradicts our problem setting. Thus, we exclude multi-agent RL baselines.

We follow previous work (Ruan et al. 2020) and use average daily crowd coverage (ADCC) to assess model performance. Each method is run 5 times, and we report the average ADCC value along with the variance. The notation Δ indicates the relative improvement of ADCC over the EADS approach under varying initial energy E .

Implementation Details. The baseline methods are implemented in Python, with training conducted using PyTorch 2.1.3 on a single NVIDIA GeForce RTX 3090 GPU. The Adam optimizer is used with a batch size of 16, an initial learning rate of 0.05, and a hidden size of 32. Each agent’s capacity is set to 10, and the number of resources is also set to 10 to assess system collaboration. The energy limit is explored within the range of 30 to 60.

Model Comparison

In this section, we compare the performance of GSTRL with existing baselines in terms of ADCC, using two real-world datasets as shown in **Table 1**. Our model consistently outperforms all baselines under varying initial energy E , achieving an improvement of 3% to 26% in ADCC on the Happy Valley dataset, and 0.4% to 40% on the TaxiBJ dataset. This demonstrates the effectiveness of our method in tackling the CPRA problem in scenarios of different scales.

As the initial energy E increases, we observe a general upward trend in the ADCC for all algorithms across both datasets. This is because higher energy expands the exploration space for public resources, allowing them to discover solutions closer to the global optimum for the entire region. This applies to both dynamic adjustment strategies in heuristic algorithms and RL methods.

Additionally, for the Happy Valley dataset, when E reaches a certain level (e.g., $E = 50$), the increase in ADCC

	Method	Algorithms	#Param(K)	E=30		E=40		E=50		E=60	
				ADCC \uparrow	$\Delta \uparrow$	ADCC \uparrow	$\Delta \uparrow$	ADCC \uparrow	$\Delta \uparrow$	ADCC \uparrow	$\Delta \uparrow$
Happy Valley	Heuristic	Static	-	1,566	-14%	1,673	-20%	2,076	-17%	2,106	-13%
		BB	-	1,717	-6%	1,686	-20%	2,128	-15%	2,235	-8%
		MYOPIC	-	1,756	-4%	1,789	-15%	2,206	-12%	2,289	-6%
		EADS	-	1,831	-	2,096	-	2,493	-	2,432	-
	RL	REINFORCE	211	1,936 \pm 8	6%	2,181 \pm 3	4%	2,239 \pm 5	-10%	2,103 \pm 10	-14%
		PPO	220	1,956 \pm 5	7%	2,203 \pm 2	5%	2,336 \pm 3	-6%	2,167 \pm 7	-11%
		SAC	220	1,963 \pm 5	7%	2,365 \pm 3	13%	2,396 \pm 3	-4%	2,196 \pm 6	-14%
		HEM	20	1,657 \pm 5	-10%	1,896 \pm 6	-10%	2,136 \pm 10	-14%	2,176 \pm 6	-11%
		GSTRL (ours)	216	2,298\pm16	26%	2,530\pm5	20%	2,585\pm8	4%	2,517\pm23	3%

	Method	Algorithms	#Param(K)	E=30		E=40		E=50		E=60	
				ADCC \uparrow	$\Delta \uparrow$						
TaxiBJ	Heuristic	Static	-	19.3	-92%	19.3	-92%	19.3	-92%	19.3	-92%
		MYOPIC	-	19.3	-92%	19.3	-92%	19.3	-92%	19.3	-92%
		EADS	-	<u>258</u>	-	<u>242</u>	-	<u>238</u>	-	<u>242</u>	-
	RL	REINFORCE	669	223 \pm 6	-14%	230 \pm 2	-15%	285 \pm 5	20%	296 \pm 6	22%
		PPO	691	229 \pm 3	-11%	241 \pm 2	-0.4%	293 \pm 2	23%	302 \pm 6	25%
		SAC	697	230 \pm 5	-11%	246 \pm 2	2%	295 \pm 3	24%	305 \pm 6	26%
		HEM	60	190 \pm 3	-26%	197 \pm 2	-19%	256 \pm 6	8%	273 \pm 5	13%
		GSTRL (ours)	685	259\pm2	0.4%	260\pm5	7%	313\pm2	32%	338\pm6	40%

Table 1: Model comparison on the Happy Valley and TaxiBJ datasets. The Δ represents the improvements in ADCC compared to the EADS approach. Bold and underlined digits are the best and EADS approach values.

Variant	Happy Valley			TaxiBJ		
	E=30	E=40	E=50	E=30	E=40	E=50
w/o AE	2,016	2,021	2,121	217	219	257
w/o S	1,272	1,372	1,385	139	141	167
w/o T	2,158	2,216	2,300	227	228	273
w/o PF	1,982	2,046	2,165	225	213	262
w/o EM	136	368	551	89	106	130
GSTRL	2,298	2,530	2,585	259	260	313

Table 2: Ablation Study Results.

slows down, and the gap between our GSTRL method and other baselines narrows. This is because the limited spatial scope of the dataset means that at $E = 50$, most resources can already cover the entire area.

In contrast, for the TaxiBJ dataset, most RL methods show significant performance improvement as E increases. However, heuristic algorithms perform poorly, with MYOPIC degenerating into the Static algorithm and EADS’s performance gradually declining as E increases. This is due to the larger spatial scale, higher grid size, and greater complexity of the TaxiBJ dataset, which allows RL methods to demonstrate better exploration strategies, while heuristic algorithms tend to get stuck in local optima.

Ablation Study

To assess the impact of each component on the performance of GSTRL, we perform ablation studies on two datasets.

Effects of Feature Learning. To evaluate the effectiveness of components for feature learning, we conduct ablation studies by removing three key components: a) **Agent Embedding (w/o AE)**: the module that encodes agent-specific characteristics into the state representation. b) **Spatial Component (w/o S)**: the spatial feature extractor for modeling the geographical dynamics of crowd flows. c) **Temporal Component (w/o T)**: the module that captures the temporal dynamics of crowd flows. As shown in **Table 2**, the ab-

sence of any component leads to a decline in performance, confirming their necessity in learning robust spatio-temporal representations of both crowd flows and public resources.

Effects of Potential Function (w/o PF). We perform the ablation of the potential function by modifying the reward design, changing it from the potential-based reward to the maximum utility among all agents. As shown in **Table 2**, removing this component leads to a significant performance drop, highlighting its role in guiding effective learning.

Effects of Exceed Mask (w/o EM). The exceed mask is designed to prevent the GSTRL training from converging to suboptimal solutions, where a large number of agents crowd into a single grid because of the highly uneven distribution of crowd flow. As shown in **Table 2**, removing the exceed mask leads to a sharp performance drop across, demonstrating its contribution to ensuring effective training of GSTRL.

Spatio-Temporal Dynamics Analysis

To evaluate the ability of the spatial-temporal feature extraction module, we design five GSTRL variants by replacing this module. These include state-of-the-art models for spatio-temporal prediction, such as SIMVP (Tan et al. 2024), which excels on grid-based data, and STDMAE (Gao et al. 2024), which is designed for graph-structured data.

As shown in **Fig. 3**, GSTRL outperforms all variants across different initial energies. We attribute this to two main factors: a) Our data is grid-based, and adapting graph-based methods requires constructing an adjacency matrix, which can distort the intrinsic spatial characteristics of the grid. b) Compared to SIMVP, which extracts spatio-temporal features holistically, our module aggregates features at each time step. Given the structurally simple yet highly time-varying nature of crowd flow, this aggregation proves more effective, despite relying on classical components.

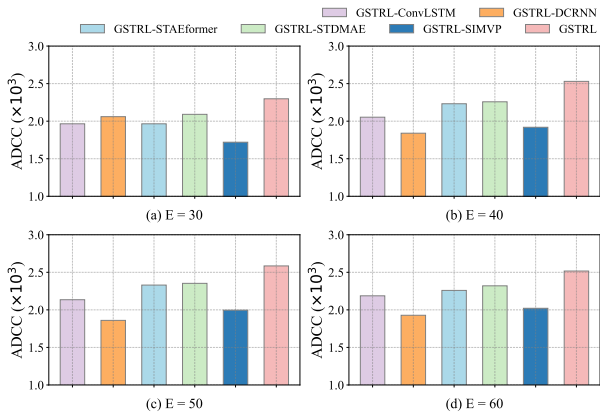


Figure 3: ADCC on different GSTRL variants.

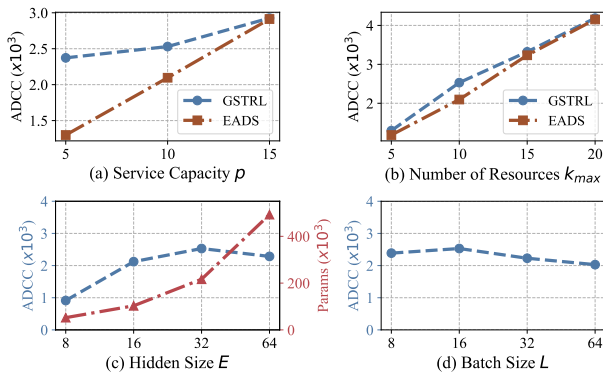


Figure 4: ADCC on different hidden sizes and batch sizes.

Hyperparameters Study

In this subsection, we evaluate the effectiveness of GSTRL using the Happy Valley dataset under different hyperparameters, which consist of model parameters and network parameters. The initial energy is set to 40. EADS, the state-of-the-art baseline for this dataset, is used for comparison.

Service Capacity. Fig. 4 (a) illustrates how ADCC varies with different service capacities. As the service capacity increases, the performance gap between EADS and GSTRL has narrowed. However, when the service capacity is low, GSTRL significantly outperforms EADS, highlighting its advantage in multi-agent collaboration.

Number of Resources. Fig. 4 (b) presents the ADCC for different numbers of resources. As shown, GSTRL outperforms EADS across all configurations. Furthermore, increasing the number of resources leads to greater ADCC, as more locations can be served simultaneously.

Hidden Size and Batch Size. We investigate the impact of hidden size and batch size, with a service capacity of 10 and 10 resources. Fig. 4 (c) reveals that a small hidden size reduces performance, and a hidden size of 64 achieves comparable performance but incurs higher computational cost.

In Fig. 4 (d), we examine the impact of batch size. The trend shows that increasing the batch size from 8 to 16 leads to improved performance, while increasing from 16 to 32 causes a slight decline, which suggests that a batch size of 16 may be optimal. The curve exhibits a smooth overall trend,

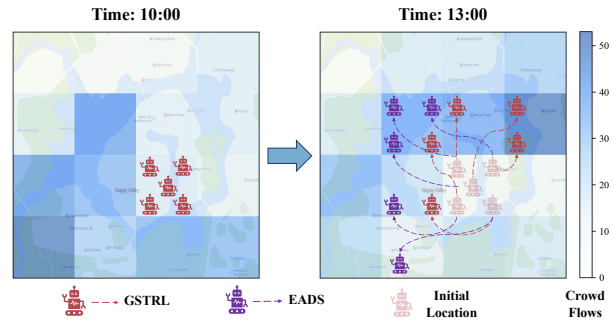


Figure 5: Strategies visualization of GSTRL compared with EADS in Happy Valley dataset.

indicating that GSTRL is relatively insensitive to variations in batch size, highlighting its strong robustness.

Case Study

In order to evaluate the explainability of our system, we perform the allocation and visualize the process from 10:00 AM to 1:00 PM on September 13, 2018. To provide a more intuitive view, we merge the grid cells into a 4x4 grid with unequal grid dimensions and plot a heat map based on the maximum crowd flow within the merged cells. The study is conducted with 5 resources, a service capacity of 10, and an energy limit of 40. We compare GSTRL with the state-of-the-art EADS baseline on the Happy Valley dataset. As shown in Fig. 5, the process begins at 10:00 AM with five resources from the resource depot. By 1:00 PM, resources allocated using GSTRL are placed in areas of higher crowd density compared to those allocated with EADS. The visualization results clearly demonstrate the superior performance of GSTRL on the CPRA problem. In addition, we developed a CPRA system and visualized the deployment of GSTRL on the TaxiBJ dataset, as detailed in Appendix.

Related Work

Dynamic public resource allocation has been extensively studied in urban computing. Many studies focus on context-specific settings, such as ambulance deployment (Ji et al. 2019) and electric bus scheduling (Yan et al. 2024). Although early heuristic algorithms, such as (Bertsimas et al. 2019) and (Zhao et al. 2019), offer basic solutions, they often perform well in constrained settings, and cannot adequately capture the dynamics of crowd flow on both spatial and temporal domains. Recent approaches (Mohammed et al. 2022; Ruan et al. 2020) incorporate real-time information for more adaptive scheduling, yet still lack consideration of future rewards, leading to suboptimal performance throughout the time horizon of the system. RL provides a powerful framework for optimizing long-term discounted return, with algorithms such as HEM (Wang et al. 2024), and SAC (Zheng, Kurt, and Wang 2024) being widely used in dynamic public resource allocation. However, in real-world scenarios, because of the limited service capacity of public resources and the strong spatio-temporal heterogeneity of crowd flows, densely concentrated flow in a specific region often requires coordinated service from multiple resources. Current RL approaches frequently converge to suboptimal solutions due to this complex decision space. To address these limitations,

we propose GSTRL, which employs potential game theory to model the state transitions of resources, and integrates related modules to capture system dynamics, so as to achieve near-global optimal decisions for CPRA.

Conclusion and Future Work

In this paper, we introduce the CPRA problem and model it as a potential game with a potential function to align individual utilities with global outcomes. We propose a GSTRL framework to solve this problem, which incorporates initial state embedding, spatio-temporal feature extraction, and related modules to capture the dynamics of the system. Extensive experiments on two real-world datasets demonstrate the superiority of GSTRL over baselines across varying parameter settings and the positive impact of its key components. In future work, we aim to optimize energy consumption and explore more on-policy learning scenarios jointly.

References

- Bertsimas, D.; et al. 2019. Emergency response optimization with robust optimization techniques. *INFORMS Journal on Optimization*, 1(1): 101–127.
- Feng, Z.; and Xiao, R. 2024. Three-dimensional task allocation for smart transportation in spatial crowdsourcing: An intelligent role division approach. *Advanced Engineering Informatics*, 62: 102736.
- Gao, H.; Jiang, R.; Dong, Z.; Deng, J.; Ma, Y.; and Song, X. 2024. Spatial-Temporal-Decoupled Masked Pre-training for Spatiotemporal Forecasting. In Larson, K., ed., *Proceedings of the Thirty-Third International Joint Conference on Artificial Intelligence, IJCAI-24*, 3998–4006. International Joint Conferences on Artificial Intelligence Organization. Main Track.
- Hu, J.; Hu, Y.; Chen, W.; Jin, M.; Pan, S.; Wen, Q.; and Liang, Y. 2024a. Attractor Memory for Long-Term Time Series Forecasting: A Chaos Perspective. arXiv:2402.11463.
- Hu, J.; Lan, D.; Zhou, Z.; Wen, Q.; and Liang, Y. 2024b. Time-SSM: Simplifying and Unifying State Space Models for Time Series Forecasting. arXiv:2405.16312.
- Ji, S.; Zheng, Y.; and Li, T. 2016. Urban sensing based on human mobility. In *Proceedings of the 2016 ACM International Joint Conference on Pervasive and Ubiquitous Computing, UbiComp '16*, 1040–1051. New York, NY, USA: Association for Computing Machinery. ISBN 9781450344616.
- Ji, S.; Zheng, Y.; Wang, Z.; and Li, T. 2019. A Deep Reinforcement Learning-Enabled Dynamic Redeployment System for Mobile Ambulances. *Proc. ACM Interact. Mob. Wearable Ubiquitous Technol.*, 3(1).
- Keneshloo, Y.; Shi, T.; Ramakrishnan, N.; and Reddy, C. K. 2019. Deep Reinforcement Learning For Sequence to Sequence Models. arXiv:1805.09461.
- Lawler, E. L.; and Wood, D. E. 1966. Branch-and-Bound Methods: A Survey. *Oper. Res.*, 14(4): 699–719.
- Li, Z.; Kovachki, N.; Azizzadenesheli, K.; Liu, B.; Bhattacharya, K.; Stuart, A.; and Anandkumar, A. 2021. Fourier Neural Operator for Parametric Partial Differential Equations. arXiv:2010.08895.
- Liang, Y.; Ouyang, K.; Yan, H.; Wang, Y.; Tong, Z.; and Zimmermann, R. 2021. Modeling Trajectories with Neural Ordinary Differential Equations. In Zhou, Z.-H., ed., *Proceedings of the Thirtieth International Joint Conference on Artificial Intelligence, IJCAI-21*, 1498–1504. International Joint Conferences on Artificial Intelligence Organization. Main Track.
- Liu, J.; Zhai, D.; Huang, W.; Ji, S.; Zhang, J.; and Li, T. 2024. Daily Schedule Recommendation in Urban Life Based on Deep Reinforcement Learning. *IEEE Transactions on Neural Networks and Learning Systems*, 1–10.
- Liu, Y.; Wu, F.; Lyu, C.; Li, S.; Ye, J.; and Qu, X. 2022. Deep dispatching: A deep reinforcement learning approach for vehicle dispatching on online ride-hailing platform. *Transportation Research Part E: Logistics and Transportation Review*, 161: 102694.
- Lv, D.; Wang, Y.; Wang, L.; Fei, Y.; Wang, K.; and Qu, X. 2024. Modular flying vehicles: Scheduling modes, social benefits, and challenges. *Communications in Transportation Research*, 4: 100144.
- Mao, X.; Wen, H.; Zhang, H.; Wan, H.; Wu, L.; Zheng, J.; Hu, H.; and Lin, Y. 2023. DRL4Route: A Deep Reinforcement Learning Framework for Pick-up and Delivery Route Prediction. In *Proceedings of the 29th ACM SIGKDD Conference on Knowledge Discovery and Data Mining, KDD '23*, 4628–4637. New York, NY, USA: Association for Computing Machinery. ISBN 9798400701030.
- Mohammed, F.; et al. 2022. Dynamic public resource allocation for disaster response. *ACM Transactions on Spatial Algorithms and Systems*, 8(1): 1–25.
- Qi, H.; Huang, D.; Zhu, Y.; Huang, D.; and Wang, H. 2023. Mini-batch Gradient Descent with Buffer. arXiv:2312.08728.
- Ruan, S.; Bao, J.; Liang, Y.; Li, R.; He, T.; Meng, C.; Li, Y.; Wu, Y.; and Zheng, Y. 2020. Dynamic Public Resource Allocation Based on Human Mobility Prediction. *Proc. ACM Interact. Mob. Wearable Ubiquitous Technol.*, 4(1).
- Sadeghi Eshkevari, S.; Tang, X.; Qin, Z.; Mei, J.; Zhang, C.; Meng, Q.; and Xu, J. 2022. Reinforcement Learning in the Wild: Scalable RL Dispatching Algorithm Deployed in Ridehailing Marketplace. In *Proceedings of the 28th ACM SIGKDD Conference on Knowledge Discovery and Data Mining, KDD '22*, 3838–3848. New York, NY, USA: Association for Computing Machinery. ISBN 9781450393850.
- Schuster, M.; and Paliwal, K. 1997. Bidirectional recurrent neural networks. *IEEE Transactions on Signal Processing*, 45(11): 2673–2681.
- Tan, C.; Gao, Z.; Li, S.; and Li, S. Z. 2024. SimVPv2: Towards Simple yet Powerful Spatiotemporal Predictive Learning. arXiv:2211.12509.
- Wang, H.; Liu, C. H.; Dai, Z.; Tang, J.; and Wang, G. 2021. Energy-Efficient 3D Vehicular Crowdsourcing for Disaster Response by Distributed Deep Reinforcement Learning. In *Proceedings of the 27th ACM SIGKDD Conference on Knowledge Discovery & Data Mining, KDD '21*,

3679–3687. New York, NY, USA: Association for Computing Machinery. ISBN 9781450383325.

Wang, J.; Wang, Z.; Li, X.; Kuang, Y.; Shi, Z.; Zhu, F.; Yuan, M.; Zeng, J.; Zhang, Y.; and Wu, F. 2024. Learning to Cut via Hierarchical Sequence/Set Model for Efficient Mixed-Integer Programming. *IEEE Transactions on Pattern Analysis and Machine Intelligence*, 46(12): 9697–9713.

Wang, Q.; Xia, Y.; ZHong, S.; Li, W.; Wu, Y.; Cheng, S.; Zhang, J.; Zheng, Y.; and Liang, Y. 2025. AirRadar: Inferring Nationwide Air Quality in China with Deep Neural Networks. arXiv:2501.13141.

Yan, Y.; Wen, H.; Deng, Y.; Chow, A. H.; Wu, Q.; and Kuo, Y.-H. 2024. A mixed-integer programming-based Q-learning approach for electric bus scheduling with multiple termini and service routes. *Transportation Research Part C: Emerging Technologies*, 162: 104570.

Yang, Z.; Jin, H.; Fan, G.; Lu, M.; Liu, Y.; Yue, X.; Pan, H.; Xu, Z.; Wu, G.; Li, Q.; Wang, X.; and Guo, J. 2024. Rethinking Order Dispatching in Online Ride-Hailing Platforms. In *Proceedings of the 30th ACM SIGKDD Conference on Knowledge Discovery and Data Mining, KDD '24*, 3863–3873. New York, NY, USA: Association for Computing Machinery. ISBN 9798400704901.

Zhang, J.; Kim, J.; O’Donoghue, B.; and Boyd, S. 2020. Sample Efficient Reinforcement Learning with REINFORCE. arXiv:2010.11364.

Zhang, J.; Zheng, Y.; and Qi, D. 2017. Deep spatio-temporal residual networks for citywide crowd flows prediction. In *Proceedings of the AAAI conference on artificial intelligence*, volume 31.

Zhao, L.; et al. 2019. Adaptive mobility service optimization using real-time traffic data. *Transportation Research Part C: Emerging Technologies*, 102: 1–20.

Zheng, J.; Kurt, M. N.; and Wang, X. 2024. Stochastic Integrated Actor–Critic for Deep Reinforcement Learning. *IEEE Transactions on Neural Networks and Learning Systems*, 35(5): 6654–6666.

Zhu, Q.; Zheng, J.; and Jamalipour, A. 2025. Deep Reinforcement Learning-Based UAV Base Station Deployment for Content Delivery in Cellular IoT Networks. *IEEE Internet of Things Journal*, 12(13): 23389–23401.

Appendix

Proof of Theorem 1

Proof. To prove that problem \mathcal{P} is NP-hard, we reduce a known NP-hard problem, the Multiple Knapsack Problem (MKP), to a special case of \mathcal{P} .

Consider a special case of problem \mathcal{P} where: a) There is a single time interval, i.e., $|T| = 1$. b) Each grid cell $g_i \in G$ contains exactly one unit of crowd flow λ_i^t . c) Each public resource $m_k \in K$ corresponds to a knapsack. d) The service capacity p_k^t of each public resource corresponds to the capacity of each knapsack. e) The decision variable $u_{i,k}^t$, which indicates whether the resource m_k serves the grid cell g_i , corresponds to placing a task in the knapsack.

Under these conditions, problem \mathcal{P} reduces to selecting a subset of tasks to maximize the objective $\sum_{i \in G} \min\{\lambda_i^t, p_k^t\}$ while satisfying the capacity constraint $\sum_{i \in G} u_{i,k}^t \leq p_k^t$. This mirrors the structure of the Multiple Knapsack Problem, where the goal is to maximize the value of selected items under multiple capacity constraints.

Since the Multiple Knapsack Problem is NP-hard, and the special case of \mathcal{P} is equivalent to MKP, it follows that \mathcal{P} is at least as hard as the Multiple Knapsack Problem. Hence, \mathcal{P} is NP-hard. \square

Proof of Theorem 3

Proof. Since G is a finite potential game and the potential function $\Phi(\zeta)$ is bounded over the finite strategy space \mathcal{S} , there exists a strategy profile ζ^* that maximizes Φ :

$$\zeta^* = \arg \max_{\zeta \in \mathcal{S}} \Phi(\zeta).$$

At ζ^* , no resource m_k can change its strategy to increase its utility, as such a change would increase Φ , contradicting the minimality of $\Phi(\zeta^*)$. Therefore, ζ^* is a pure-strategy Nash equilibrium. \square

BiLSTM Gating Mechanism

In the main text (Subsection Spatio-Temporal Feature Extraction), we introduced a Bidirectional LSTM (BiLSTM) to capture temporal patterns. Here, we provide the detailed gating equations for each step in the forward pass. The backward pass follows the same formulation in reverse order.

Forward LSTM.

- **Forget Gate.** Determines which information to remove from the cell state:

$$F_t = \sigma(W_f \cdot [H_{t-1}, X_t] + b_f). \quad (11)$$

- **Input Gate and Candidate Cell State.** Selects which values to add to the cell state:

$$I_t = \sigma(W_i \cdot [H_{t-1}, X_t] + b_i), \quad (12)$$

$$\tilde{C}_t = \tanh(W_C \cdot [H_{t-1}, X_t] + b_C). \quad (13)$$

- **Cell State Update.** Combines the old cell state (filtered by F_t) with newly arrived information (filtered by I_t):

$$C_t = F_t \cdot C_{t-1} + I_t \cdot \tilde{C}_t. \quad (14)$$

- **Output Gate.** Generates the final hidden state at step t :

$$O_t = \sigma(W_o \cdot [H_{t-1}, X_t] + b_o), \quad (15)$$

$$H_t = O_t \cdot \tanh(C_t), \quad (16)$$

where X_t is the input at time t , H_{t-1} is the previous hidden state, C_{t-1} is the previous cell state, $\sigma(\cdot)$ is the sigmoid activation, and $\tanh(\cdot)$ is the hyperbolic tangent. W_f, W_i, W_C, W_o and b_f, b_i, b_C, b_o are learnable parameters.

Backward LSTM. For the backward pass, the same gating operations (11)–(16) apply, but the sequence is processed in reverse order, i.e., from t_{\max} down to t_{\min} . The final BiLSTM hidden state at time t is the concatenation (or sum) of forward and backward hidden states:

$$T_t = \vec{H}_t + \overleftarrow{H}_t. \quad (17)$$

Hence, the BiLSTM captures both past and future contexts, providing enhanced temporal representations for resource allocation decisions.

Algorithm 1: GSTRL Algorithm

Input: Input sets of each public resource’s state M_t , and sets of predicted crowd flow’s amount G_t . The actor network with parameters θ_a , and the critic network with parameters θ_c .

Output: Trained actor network parameter θ_a^* .

- 1: Randomly initialize θ_a and θ_c .
 - 2: Initialize replay buffer \mathcal{B} .
 - 3: **for** episodes $k = 0, 1, 2, \dots, EPI_{max}$ **do**
 - 4: Generate the action a_t according to π_{θ_a} .
 - 5: Execute the action a_t and obtain s_t and r_t .
 - 6: Store (s_t, a_t, s_{t+1}, r_t) into replay buffer \mathcal{B} .
 - 7: Randomly sample M samples from the replay buffer of length N .
 - 8: **for** $t = 0, 1, 2, \dots, t_{max}$ **do**
 - 9: **for** $k = 0, 1, 2, \dots, k_{max}$ **do**
 - 10: Calculate the expected reward.
 - 11: Compute the Q-value $Q_{\pi_{\theta_a}}(s_t, a_t)$ based on the samples.
 - 12: Compute Advantage $L(\omega)$ based on Eq. (21).
 - 13: **end for**
 - 14: **end for**
 - 15: Compute the loss of critic \mathcal{L}_{θ_c} based on Eq. (8).
 - 16: Compute the loss of policy \mathcal{L}_{θ_a} based on Eq. (9).
 - 17: Calculate the joint loss $\mathcal{L}_{\theta_{ac}}$ based on Eq. (10).
 - 18: Update the parameters of the actor-critic model.
 - 19: **end for**
 - 20: **return** $\theta_a^* = \theta_a$.
-

Value Functions and Advantage

Given a policy π_{θ_a} , we define the state-action function $Q_{\pi_{\theta_a}}(s_t, a_t)$ and the state-value function $V_{\pi_{\theta_a}}(s_t)$ as:

$$Q_{\pi_{\theta_a}}(s_t, a_t) = \mathbb{E}_{\pi_{\theta_a}}[r_t \mid s = s_t, a = a_t], \quad (18)$$

$$V_{\pi_{\theta_a}}(s_t) = \mathbb{E}_{a_t \sim \pi_{\theta_a}(s_t)}[Q_{\pi_{\theta_a}}(s_t, a_t)]. \quad (19)$$

The estimated value function is subsequently used to compute the advantage function $A_{\pi_{\theta_a}}(s_t, a_t)$:

$$A_{\pi_{\theta_a}}(s_t, a_t) = Q_{\pi_{\theta_a}}(s_t, a_t) - V_{\pi_{\theta_a}}(s_t). \quad (20)$$

The advantage function reflects how much better (or worse) taking action a_t in state s_t is compared to the average action. To expedite computation, we approximate it as follows (Keshnloo et al. 2019):

$$A_{\pi_{\theta_a}}(s_t, a_t) \approx r_t + \gamma V_{\pi_{\theta_a}}(s_{t+1}) - V_{\pi_{\theta_a}}(s_t). \quad (21)$$

Algorithm

The algorithmic process of the proposed GSTRL algorithm is listed in Algorithm 1.

Real-World Deployment Visualization

To provide an intuitive view of the behavior of GSTRL in practice, we perform a deployment visualization on TaxiBJ. We first aligned the recorded flow counts and their geographic coordinates with a real map of Beijing and rendered time-varying heatmap. Public resources are modeled as unmanned aerial vehicles (UAVs) unconstrained by the road network, and the study scenario is framed as drone delivery units that can respond directly to crowd demand. Throughout this study, we fix the initial energy to 40, deploy 50 public resources, and set their service capacity to 10.

Using the trained GSTRL, we replay the test period from March 22 to March 31, 2016 and record the location of each public resource at each time step. **Fig. 6** overlays their locations on the heatmap. As the demand distribution changes over time, most UAVs migrate visibly to the densest regions, highlighting the superior performance of GSTRL. We also plot the remaining energy and service capacity traces for each public resource, confirming that the policy satisfies two constraints of CPRA, every UAV retains sufficient energy to return to the resource depot at the end of each day and the service capacity remains constant over time. Our source codes are available in the supplementary materials.

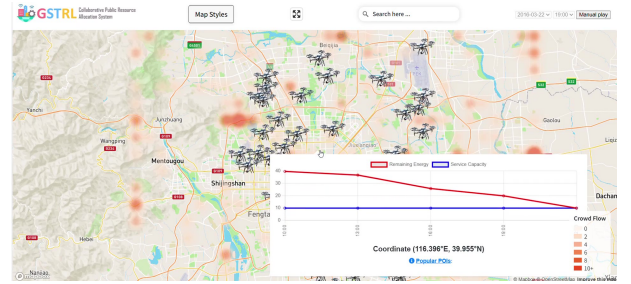


Figure 6: Web platform of CPRA system.